STEM CELLS®

EMBRYONIC STEM CELLS/INDUCED PLURIPOTENT STEM CELLS

Distinct Responses of Stem Cells to Telomere Uncapping—A Potential Strategy to Improve the Safety of Cell Therapy

CHANG CHING LIU,[a] DONG LIANG MA,[b,c] TING-DONG YAN,[a] XIUBO FAN,[a,d] ZHIYONG POON,[e] LAI-FONG POON,[a] SU-ANN GOH,[a] STEVE G. ROZEN,[a] WILLIAM YING KHEE HWANG,[a,d] VINAY TERGAONKAR,[f,g,i] PATRICK TAN,[a] SUJOY GHOSH,[h] DAVID M. VIRSHUP,[a] EYLEEN L. K. GOH,[b,c,j,k] SHANG LI[a,j]

Key Words. Stem cell transplantation • Telomerase • Telomere • Pluripotent stem cells • Malignancy • Cellular therapy

[a]Cancer and Stem Cell Biology Programme, [b]Neuroscience Academic Clinical Programme, [h]Cardiovascular and Metabolic Disorders Programme, Duke-NUS Medical School, Singapore; [c]Department of Research, National Neuroscience Institute, Singapore; [d]Department of Hematology, Singapore General Hospital, Singapore; [e]BioSystems and Micromechanics, , Singapore-MIT Alliance for Research & Technology, Singapore; [f]Division of Cancer Genetics and Therapeutics, Institute of Molecular and Cell Biology (IMCB), Singapore; [g]Department of Biochemistry, [j]Department of Physiology, Yong Loo Lin School of Medicine, National University of Singapore, Singapore; [i]Centre for Cancer Biology, University of South Australia and SA Pathology, Adelaide, Australia; [k]KK Women's and Children's Hospital, KK Research Center, Singapore

Correspondence: Shang Li, M.D., Ph.D., Cancer and Stem Cell Biology Programme, Duke-NUS Medical School, 169857, Singapore. Telephone: (65) 6601 1259; Fax: (65) 6221 2402; e-mail: shang.li@duke-nus.edu.sg

C.C.L., D.L.M., and T.-D.Y. contributed equally to this article.

Received October 14, 2015; accepted for publication May 14, 2016; first published online in STEM CELLS *EXPRESS* June 14, 2016.

1066-5099/2016/$30.00/0

http://dx.doi.org/10.1002/stem.2431

ABSTRACT

In most human somatic cells, the lack of telomerase activity results in progressive telomere shortening during each cell division. Eventually, DNA damage responses triggered by critically short telomeres induce an irreversible cell cycle arrest termed replicative senescence. However, the cellular responses of human pluripotent stem cells to telomere uncapping remain unknown. We generated telomerase knockout human embryonic stem (ES) cells through gene targeting. Telomerase inactivation in ES cells results in progressive telomere shortening. Telomere DNA damage in ES cells and neural progenitor cells induces rapid apoptosis when telomeres are uncapped, in contrast to fibroblast cells that enter a state of replicative senescence. Significantly, telomerase inactivation limits the proliferation capacity of human ES cells without affecting their pluripotency. By targeting telomerase activity, we can functionally separate the two unique properties of human pluripotent stem cells, namely unlimited self-renewal and pluripotency. We show that the potential of ES cells to form teratomas in vivo is dictated by their telomere length. By controlling telomere length of ES cells through telomerase inactivation, we can inhibit teratoma formation and potentially improve the safety of cell therapies involving terminally differentiated cells as well as specific progenitor cells that do not require sustained cellular proliferation in vivo, and thus sustained telomerase activity. STEM CELLS *2016; 00:000–000*

SIGNIFICANCE STATEMENT

The ability of pluripotent stem cells to self-renew and to differentiate into various cell types of all three germ layers has provided a great source for cell therapy in humans. However, their ability to proliferate continuously also raises concerns of tumor formation in vivo. Our studies demonstrate that the telomerase is dispensable for the pluripotency of embryonic stem cells. By controlling telomere length through inactivation of telomerase, we can inhibit teratoma formation and greatly improve the safety of cell therapies. Our works provide a potential new strategy that may reduce, if not eliminate, tumorigenicity of stem cells during cell therapy.

INTRODUCTION

Human chromosome ends are capped by telomeres that contain long six-nucleotide DNA repeats 5′-TTAGGG-3 with single stranded 3′ G-rich overhangs [1]. The telomeric DNA repeats are bound by shelterin protein complexes consisting of TRF1, TRF2, RAP1, TIN2, TPP1, and POT1 that distinguish naturally occurring chromosomal ends from DNA double-strand breaks. Therefore, telomeres are essential for cell genomic stability. Telomeric repeat sequences are synthesized by telomerase, a reverse transcriptase. The human core telomerase contains at least two essential subunits, the protein subunit, hTERT, and the RNA subunit, hTR, [2, 3]. While *hTR* is widely expressed, *hTERT* and, consequently, telomerase activity, is barely detected in most human adult somatic tissues, except germ cells and some stem cells [2–6]. Because of the lack of telomerase activity in somatic cells, about 50-200 bp of telomeric DNA repeats are lost during each cell division [7, 8]. Progressive telomere shortening may function as an internal clock that determines the replicative capacity of normal human somatic cells [9]. When telomeres shorten to a critical limit, they become

uncapped. This triggers ATM- and/or ATR-dependent DNA damage signaling cascades. Through the downstream transducer kinases CHK2 and CHK1, the uncapped chromosome ends are marked by proteins involved in DNA damage response, such as 53BP1, NBS1 and γ-H2AX, and form cytologically distinct telomere dysfunction-induced foci (TIFs) [10]. This is different from telomere-associated foci that can arise from anywhere in the telomere [11, 12]. As few as five dysfunctional telomeres are sufficient to trigger irreversible cell cycle arrest, termed replicative senescence, in primary human fibroblast cells [13–15]. Such cells at senescent state are metabolically active and arrest at G1 phase. They show enlarged cell morphology, β-galactosidase induction, as well as a senescence-associated secretory phenotype [16]. The induction of replicative senescence is dependent on functional p53 and pRB, as inactivation of these two pathways leads to the escape of senescence [17]. One p53 target-p21 is upregulated during replicative senescence and plays a pivotal role in cell cycle arrest at the G1 phase, as p21 inactivation can postpone the onset of senescence [18]. Previous studies proposed that progressive telomere shortening in normal human somatic cells leads to an intermediate–state telomere structure in which the chromosome end triggers the DNA damage response, while preventing the occurrence of chromosome end-to-end fusion [15, 19]. Such a model predicts persistent activation of the DNA damage response, since dysfunctional telomeres are irreparable [11, 12].

Recent studies link telomere dysfunction to diverse degenerative diseases and premature aging. While telomere length in embryonic stem (ES) cells and germ cells is sustained, the telomerase activity in tissue-specific progenitor/stem cells is not sufficient for complete telomere maintenance [20]. As a result, the telomere length in tissue-specific progenitor/stem cells shortens progressively. This length decrease eventually leads to telomere uncapping and induction of ATM- and/or ATR-dependent DNA damage signaling cascades, which limit the proliferation capacity of tissue-specific progenitor/stem cells [21]. Consistent with these findings, heterozygous mutations in dyskerin, *hTR*, and *hTERT*, as well as other telomere maintenance genes, are found in patients with premature aging suffering from conditions, such as dyskeratosis congenita, aplastic anemia, myelodysplastic syndrome, and idiopathic pulmonary fibrosis [22]. The telomerase knockout mouse model facilitates investigations into telomere dysfunction-mediated diseases and shows remarkable similarity to the human disease phenotypes [23–25]. However, the cellular responses of human stem cells and progenitor cells to dysfunctional telomeres have not been characterized in detail.

Cell types respond distinctively to various types of DNA damage ranging from cell cycle arrest and senescence to apoptosis. ES cells and induced pluripotent stem (iPS) cells are particularly sensitive to DNA damage-induced apoptosis [26–29]. Such a mechanism may eliminate damaged cells to prevent compromising genomic integrity and tumorigenicity in humans. Several distinct properties of ES cells and iPS cells may regulate pluripotent stem cell responses to DNA damage: (a) differential activation of p53 transcriptional targets and p53 interacting cytoplasmic partners, (b) high mitochondria priming or readiness for apoptosis due to the balance between pro-apoptotic and anti-apoptotic proteins shifting closer to the apoptotic threshold [30], and (c) an abbreviated G1 phase [31]. Conversely, adult stem cells are more resistant to DNA damage-induced apoptosis, although such resistance may compromise genomic instability, when DNA damage-induced mutations are not properly repaired [32]. Understanding how pluripotent and adult stem cells regulate cellular responses to DNA damage, as well as their biological roles in vivo, remains limited. Previous studies determined that within two days following induction of human ES cell differentiation through embryoid body (EB) formation, partially differentiated cells become resistant against DNA damage-induced apoptosis [31].

To investigate the cellular responses of ES and progenitor cells to telomere dysfunction, we engineered telomerase knockout human ES cells using gene targeting. We find that telomerase-null ES cells retain their pluripotency, and their potential to form teratomas in vivo is limited by their telomere length. When telomeres are shortened to a critical limit, the telomerase-null ES cells with dysfunctional telomeres undergo apoptosis rather than permanent cell cycle arrest (senescence). Telomere dysfunction also induces cellular apoptosis in partially differentiated neural progenitor cells (NPCs) distinct from the cellular responses caused by treatment with DNA damaging reagents. Therefore, by inactivating telomerase, an intrinsic pathway that is naturally silenced during cellular differentiation, we can limit the self-renewal capacity of ES cells and NPCs without affecting their pluripotency both in vitro and in vivo. Manipulating telomere length in telomerase-null ES cells permits a balance between cell proliferation capacity and tumor formation prevention. This strategy provides a novel solution that may reduce, if not eliminate, the tumorigenicity of stem cells during cell therapy.

Materials and Methods

CRISPR and Paired Zinc Finger Nucleases

The exon 1 of human *hTERT* gene was subjected to potential sgRNA target search using the online software created by Feng Zhang's group (http://tools.genome–engineering.org) [33]. The very top hits were chosen and used for the experiments hence described. The zinc finger nucleases (ZFNs) expression plasmids were ordered from Sigma-Aldrich, St. Louis, Missouri, https://www.sigmaaldrich.com (Cat# CSTZFN-1KT-hTERT).

Maintenance of H1 Human ES Cell Culture

Feeder-independent human H1 and WA018 ES cells from WiCell were grown on matrigel (BD Biosciences, Franklin Lakes, New Jersey, http://www.bd.com)-coated cell culture dishes using mTeSR1 culture medium (StemCell Technologies, Vancouver, Canada, http://www.stemcell.com). When the cells reached 80%-90% confluence, they were passaged using Dispase, and split 1:6 to 1:12 onto new matrigel-coated cell culture dishes.

Gene Targeting Using Neon Transfection System

The gene-targeting procedure was adapted from previously published protocols [34]. WA018 and H1 human ES cells were grown to 80%-90% confluence. The cells were then harvested using Accutase, and the cell number counted. The cells were washed once with 1xPBS before resuspension in Resuspension buffer (R) at 1 x 10^7 cells/ml. For every 1 x 10^7 cells in 1 ml of Resuspension buffer, 25 μg of each pCas9(D10A)- green fluorescent protein (GFP)-sgRNA plasmid was mixed with WA018

cells. About 6.25 μg of pZFN1 (GFP: green fluorescent protein) plasmid DNA, 6.25 μg of pZFN2 plasmid DNA and 37.5 μg of SacI-linearized pBSK-3kb-5′-LoxP-hTERT-FRT-PGKNeo-FRT-LoxP-3′-PGK-DTA(ΔZFN) targeting plasmid were added and mixed with H1 cells well before electroporation. For electroporation, 100 μl of the cell suspension in Resuspension buffer was electroporated using a 100 μl Neon pipette in a Neon tube containing 3 ml of Electrolytic Buffer (E2). The electroporation conditions are as follow: Pulse, V 1050, MS 30, Number 2. After the electroporation, the cells were plated onto matrigel-coated 10 cm dish in 6 ml of mTeSR1 containing 10 μM Y-27632 (Rock inhibitor). About 5-6 x 10^6 cells were plated onto one 10 cm dish. The cells were maintained in mTeSR1, and the medium was changed every day.

Screening of *hTERT* Knockout Clones in WA018

At 48 hours after electroporation, the GFP positive cells were sorted and seeded on matrigel-coated plate in mTeSR1 containing 10 μM Y-27632 to allow the emerging of single cell colonies. Fluorescent PCR-capillary gel electrophoresis was then utilized to screen for colonies with biallelic deletion in hTERT coding region [35].

Screening of G418-Resistant Targeted H1 ES Cell Clones

At 48 hours after electroporation, mTeSR1 containing 50 μg/ml G418 was added to select for G418-resistant clones. The cells were maintained in mTeSR1 containing 50 μg/ml G418 for about 12 days before the colonies were big enough for picking. When the G418-resistant colonies reached about 3-4 mm in size, the individual G418-resistant clones on the 10 cm dish were then picked using sterile P200 pipette tip and transferred onto two new wells of matrigel-coated 96-well plate. The colonies grew for 2-3 days prior to screening using PCR, as previously described [36].

Genomic DNA Extraction and Southern Blotting

Genomic DNA was extracted using Gentra Puregene Genomic DNA Purification Kit (Qiagen, Hilden, Germany, https://www.qiagen.com). Southern blots for detection of targeted genomic insertions were performed as previously described [37]. For telomerase activity analysis, telomeric repeat amplification protocol (TRAP) assay was performed as previously described [4]. For telomere length measurement, the genomic DNA was digested with HphI and MnlI at 37°C for 16 hours. The DNA blot was hybridized with ^{32}P-labeled $(TTAGGG)_6$ oligonucleotides as previously described [38].

FLP Pop-Out of PGK-Neo Selection Cassette

For FLP pop-out of PGK-Neo cassette, the cells were transiently transfected with pCAG-Flpe:GFP plasmid using Neon transfection system (as described above). The cells were maintained in mTeSR1 containing 10 μM Y-27632 for 24 hours, and GFP-positive cells were then sorted out and collected using FACS. The cells were then seeded at low density of 200-500 cells/well in a 6-well dish to allow single ES cell to form individual colony. When the colonies grew to about 3-4 mm in diameter, they were transferred to a 96-well dish and subjected to PCR diagnosis for the excision of PGK-Neo cassette.

Cre Pop-Out of *hTERT* Alleles

For Cre pop-out of *hTERT* exon 1 and exon 2, $hTERT^{+/loxP}$ and $hTERT^{loxP/loxP}$ cells were transiently transfected with pCre-IRES-mCherry plasmid using Neon transfection system (as described above). The cells were maintained in mTeSR1 containing 10 μM Y-27632 for 24 hours, the mCherry-positive cells were sorted and collected using FACS. The cells were then seeded at low density of 200-500 cells/well on a 6-well dish to allow single ES cells to form individual colonies. When the colonies grew to about 3-4 mm in diameter, they were transferred to a 96-well dish and subject to PCR diagnosis for the excision of hTERT exon 1 and exon 2.

Reset of Telomere Length in Telomerase Inducible Knockout ES Cells by Transient Overexpression of hTERT

To reset telomere lentgth in telomerase inducible knockout ES cells, an episomal vector expressing hTERT-IRES-GFP was transiently transfected into the $hTERT^{loxP/loxP}$ ES cells, after which the GFP-positive cells were FACS sorted and single cell colonies were isolated. No integration of the hTERT-IRES-GFP expression vector was detected as the single cell-derived colonies were negative for GFP expression. No integration of hTERT-IRES-GFP expression vector was further supported by the lack of telomerase activity and gradual telomere shortening in these cells upon Cre-induced deletion of endogenous hTERT.

Cell Proliferation Assay-CellTiter-Glo

Cells were seeded onto 96-well plate at a density of 1000 cells/well and cultured over a period of 7 days to monitor cell proliferation using ATP assay (CellTiter-Glo Luminescent Cell Viability Assay, Promega, Fitchburg, Wisconsin, https://www.promega.com). Luminescence was measured on a microplate reader (Infinite 200,Tecan, Mannedorf, Switzerland, www.tecan.com) every 24 hours.

Cell Proliferation assay-EdU Labeling Assay

Cell proliferation was detected through the incorporation of 10 μM EdU within an hour using Click-iT EdU Alexa Fluor 488 Imaging Kit (Thermo Fisher Scientific, Waltham, Massachusetts, www.thermofisher.com). Immunofluorescence staining was done in accordance with the protocol provided by the manufacturer.

Cell Cycle Analysis

Cells were harvested by Accutase, washed, and fixed in ice-cold 70% ethanol followed by propidium iodide (PI) staining with RNase A treatment. Cell cycle profiles were acquired on flow cytometer MACSQuant VYB (Miltenyi Biotec, Bergisch Gladbach, Germany, http://www.miltenyibiotec.com) and analyzed using ModFit LT.

Apoptosis Assay

Cells were harvested by Accutase, washed once with PBS and stained with 7-AAD and Annexin V (BD Biosciences, Franklin Lakes, New Jersey, http://www.bd.com) for 15 minutes at room temperature in the dark. Cytohistofluorescence data were acquired on flow cytometer BD LSRFortessa (BD Biosciences, Franklin Lakes, New Jersey, http://www.bd.com) and analyzed using FlowJo (Tree Star, Ashland, Oregon, www.flowjo.com).

Cellular Senescence Assay

The cellular senescence was analyzed using a β-galactosidase staining kit (Cell Signaling Technology, Danvers, Massachusetts, http://www.cellsignal.com) according to the protocol provided.

Microarray Data and Pathway Enrichment Analysis

Total RNA was extracted using NucleoSpin RNA extraction kit (Macherey-Nagel, Duren, Germany, www.mn-net.com) with on-column DNase digestion. Gene expression analysis was performed on GeneChip PrimeView human gene expression array (Affymetrix, Santa Clara, California, http://www.affymetrix.com).

Background-adjusted, quantile-normalized gene expression summaries for Affymetrix PrimeView chip data were generated via the Robust Multichip Average method [39]. Genes with a maximum average group expression of $\geq$50units were retained for downstream analysis. Detection of the major sources of variation (including sample outliers) was accomplished by principal components analysis (PCA) based on covariances (Partek Genomics Suite, v6.6). Differentially expressed genes were identified via analysis of variance, coupled with planned contrasts between relevant groups (Partek Genomics Suite, v6.6). The number of statistically significant differentially expressed genes was controlled by the false discovery rate [40]. Pathway enrichment analysis was conducted via the Gene Set Enrichment Analysis (GSEA) method [41] by comparing gene expression profiles of the relevant groups against the Kyoto Encyclopedia of Genes and Genomes (KEGG) pathway repository available from the Molecular Signature Database (MSigDB) [42]. Pathways with a false discovery rate $\leq$5% were considered to be statistically significant.

Formation of EB and Induction of Spontaneous Differentiation

Embryoid bodies were formed by plating Accutase-treated single-cell suspension onto low-adherence dishes in human ES cell culture medium. For spontaneous differentiation, 7 to 10-day old EBs were used according to previously established protocol [43]. In brief, the EBs (about 5-10) from human ES cells were transferred onto gelatin-coated 24-well plate and differentiated in DMEM + 10% fetal bovine serum (FBS) for 1-2 weeks.

Neural Induction, Neuronal and Astrocytes Differentiation

Neural induction of H1 ES cells was carried out using a previously established protocol [44]. Briefly, *hTERT*$^{+/+}$ and *hTERT*$^{-/-}$ ES cells were cultured in mTeSR1 medium. When the ES cell cultures reached ~20% confluence, mTeSR1 medium was removed and replaced with neural induction media containing DMEM/F12: Neurobasal (1:1), 1xN2, 1xB27, 1% Glutmax, 5 μg/mL BSA, 4 μM CHIR99021 (Cellagentech, San Diego, California, http://www.cellagentech.com), 3 μM SB431542 (Cellagentech), 0.1 μM Compound E (γ-Secretase Inhibitor XXI, Millipore Darmstadt, Germany, http://www.emdmillipore.com), 10 ng/mL hLIF (Millipore, Darmstadt, Germany, http://www.emdmillipore.com) for 7 days. The culture was then split 1:3 for the next six passages using Accutase, and the cells were cultured in human NPCs maintenance media containing DMEM/F12: Neurobasal (1:1), 1xN2, 1xB27, 1% Glutmax, 5 μg/mL BSA, 3 μM CHIR99021, 2 μM SB431542, 10 ng/mL hLIF on matrigel-coated plates. After six passages, the cells were split 1:10 regularly.

The human NPCs neuronal differentiation assay was performed by plating 5 x 10^4 cells/well on laminin- (37°C, 4 hours) coated 24-well plates in neural differentiation media containing DMEM/F12: Neurobasal (1:1), 1xN2, 1xB27, 1% Glutmax on pLL (4°C, overnight). After 3 days, 10 ng/mL BDNF and 10 ng/mL GDNF were added to the media every other day and cultured for another 11 days.

The human NPC to astrocyte differentiation assay was performed by plating 8 x 10^4 cells/well onto 1% Glutmax on matrigel-coated 24-well plates in neural differentiation media containing DMEM/F12: Neurobasal (1:1), 1xN2, 1% FBS.

Teratoma Formation Assay

For the teratoma assay, ES cells were harvested using Dispase, washed with 1xPBS, and resuspended in 30% matrigel (BD Biosciences, Franklin Lakes, New Jersey, http://www.bd.com). About 1 x 10^6 cells (100 μl) were injected subcutaneously into NSG mice (NOD.Cg-*Prkdc*^{scid} *Il2rg*^{tm1Wjl}/SzJ) in the dorsolateral area bilaterally as previously described [45]. About 8-9 weeks after injection, the mice were sacrificed, and the tumors were harvested.

Transplantation and Histology

Immunodeficient mice (SCID, NOD.CB17-*Prkdc*^{scid}/NcrCrl) ($n = 5$) were anaesthetized with Ketamine (85 mg/kg) plus Xylazine (10 mg/kg) and fixed in a Stoelting stereotaxic apparatus. A small hole was drilled in the skull above the intended injection sites and a syringe (1 μl, Hamilton) containing 1 μl Accutase-dissociated human ES cells (5 × 10^4 cells per μl) in PBS (pH 7.4) was lowered into the striatum at ~0.5 mm posterior to bregma, 2.0 mm lateral to midline, 3.2 mm ventral to dura. At 4, 8, or 16 weeks after transplantation, animals were deeply anaesthetized and perfused transcardially with 50 ml of saline, followed by 100 ml of 4% paraformaldehyde for 30 minutes. The 40 μm coronal sections were cut using a cryostat, and serial sections were transferred to individual wells of a 24-well tissue culture dish. Sections were incubated in blocking solution (5% normal goat serum and 0.1% Triton X-100 in TBS) for 1 hour. Subsequently, primary antibody (mouse anti-Human Nuclei, 1:500, Abcam; goat anti-DCX, 1: 500, Santa Cruz Biotechnology, Inc. Dallas, Texas, http://www.scbt.com; mouse anti-MAP2, 1:1,000, Sigma-Aldrich, St. Louis, Missouri, https://www.sigmaaldrich.com; mouse anti-NeuN, 1:500, Abcam, Cambridge, United Kingdom, www.abcam.com; mouse anti-GFAP, 1:1,000, Millipore, Darmstadt, Germany, http://www.emdmillipore.com) in blocking solution was added to the sections and incubated overnight at 4°C. After three TBS washes, sections were incubated with Alexa Fluor-conjugated secondary antibody solution for 2 hours at room temperature. Nuclei were visualized by DAPI staining (Sigma-Aldrich, St. Louis, Missouri, https://www.sigmaaldrich.com). Sections were then mounted onto the glass slide. Images were acquired on a Zeiss LSM 710 confocal microscope or LSM 7 ELYRA PS.1 system (Carl Zeiss, Pte. Ltd., Singapore, www.zeiss.com.sg).

Immunofluorescence Staining

For immunofluorescence assays, the cells were fixed in 4% paraformaldehyde for 10 minutes. The fixed cells were washed three times with 0.1 M Tris-buffered saline containing 0.1% Triton-X 100 (TBS-TX) and incubated in the following primary antibodies in blocking buffer at 4°C overnight: mouse anti-Oct3/4 (1:500, Santa Cruz Biotechnology, Inc. Dallas, Texas, http://www.scbt.com), mouse anti-Tra-1-60 (1:100, Santa Cruz Biotechnology, Inc. Dallas,

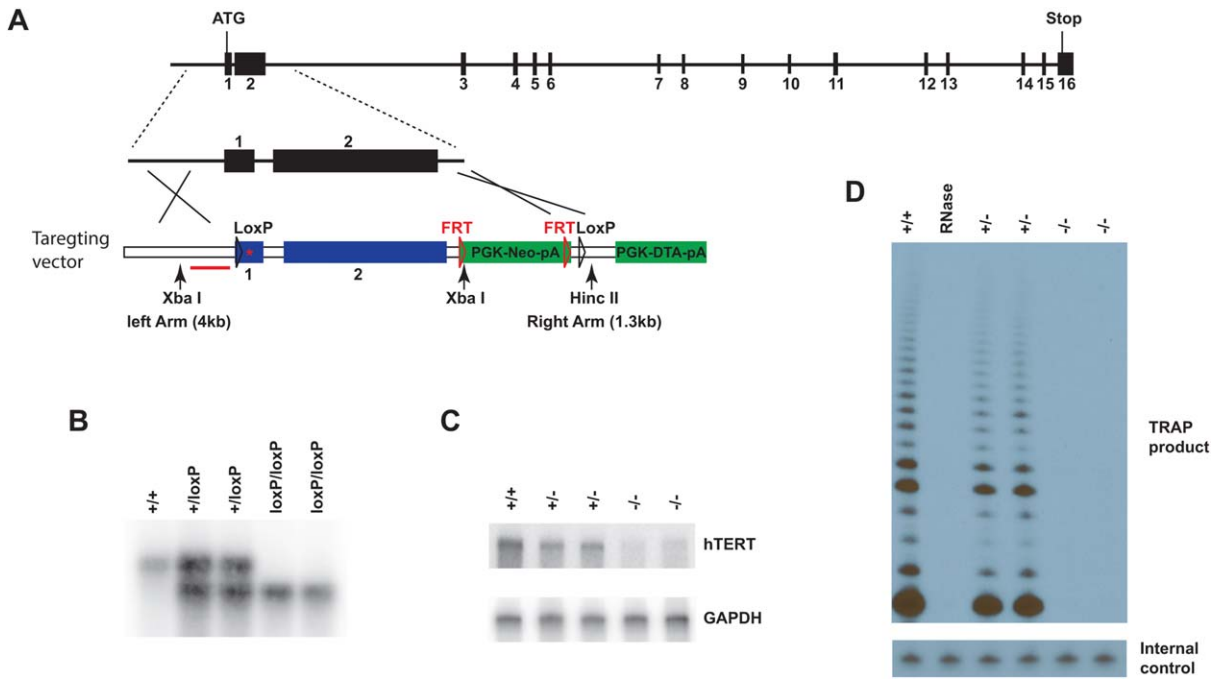

Figure 1. Engineering *hTERT* inducible knockout H1 embryonic stem (ES) cells. (A): Schematic design of the gene targeting strategy to introduce loxP sites flanking the exon 1 and exon 2 of the *hTERT* genomic locus. (B): Targeted alleles of *hTERT* are confirmed by Southern blotting analysis using genomic DNAs digested with Xba I and Hinc II restriction enzymes. The probe for Southern blotting analysis is shown in red. (C): Expression of full length *hTERT* in $hTERT^{+/+}$; $hTERT^{+/-}$, and $hTERT^{-/-}$ ES cells was analyzed by RNA protection assay (RPA) using ^{32}P-labeled radioactive RNA probe encompassing *hTERT* exon 2. (D): TRAP assay using whole cell extracts from independent $hTERT^{+/+}$; $hTERT^{+/-}$, and $hTERT^{-/-}$ clonal ES cell lines measures telomerase activity. A RNase-treated sample is used as negative control. Abbreviations: TRAP, telomeric repeat amplification protocol.

Texas, http://www.scbt.com), rabbit anti-Nanog (1:100, Cell Signaling Technology, Danvers, Massachusetts. http://www.cellsignal.com), mouse anti-SSEA-4 (1:500, Millipore, Darmstadt, Germany, http://www.emdmillipore.com), rabbit anti-AFP (1:400, Dako, Glostrup, Denmark, http://www.dako.com), mouse anti-Desmin (1:100, Abcam, Cambridge, United Kingdom. www.abcam.com); goat anti-SOX2 (1: 500, Santa Cruz Biotechnology, Inc. Dallas, Texas, http://www.scbt.com), mouse anti-SMA (1: 200, Sigma-Aldrich, St. Louis, Missouri. https://www.sigmaaldrich.com), mouse anti-Tuj1 (1:1,000, Covance, Princeton, New Jersey, www.covance.com), mouse anti-GFAP (1:1,000, Millipore, Darmstadt, Germany, http://www.emdmillipore.com), mouse anti-Human Nuclei (1:500, Abcam, Cambridge, United Kingdom, www.abcam.com), mouse anti-Nestin (1:1,000, Millipore, Darmstadt, Germany, http://www.emdmillipore.com), or goat anti-DCX (1: 500, Santa Cruz Biotechnology, Inc. Dallas, Texas, http://www.scbt.com). The following day, cells were washed with TBS-TX and incubated with Alexa Fluor-conjugated secondary antibodies (Thermo Fisher Scientific, Waltham, Massachusetts, www.thermofisher.com, 500×) in TBS-TX for two hours at room temperature. Nuclei were visualized by DAPI staining (Sigma-Aldrich, St. Louis, Missouri, https://www.sigmaaldrich.com). Images were acquired on a Zeiss LSM 710 confocal microscope or LSM 7 ELYRA PS.1 system (Carl Zeiss, Pte. Ltd., Singapore, www.zeiss.com.sg).

Results

Engineering *hTERT* Knockout ES Cells

Human telomerase contains two core components the protein catalytic subunit, hTERT, and the RNA subunit, *hTR* [2, 3]. Deletion of either *hTERT* or *hTR* resulted in the complete loss of telomerase activity in vivo as shown in mouse models [24, 46–49]. First, we used the CRISPR/Cas9 system to inactivate *hTERT* directly. As shown in Supporting Information Figure S1A, S1B, five CRISPR guide RNAs targeting *hTERT* exon 1 were designed, and all resulted in efficient, site-specific double strand breaks (DSBs). To enhance genome-editing specificity, Cas9 nickase was transfected with a pair of CRISPR guide RNAs (S2 and S3) to introduce targeted DSBs [50] illustrated in Supporting Information Figure S1C. Six independent ES cell clones derived from the WA018 ES cell line with a deletion in hTERT exon 1 were isolated using fluorescent PCR-capillary gel electrophoresis [35]. DSB-induced insertion/deletion (indel) mutations in three clones were confirmed by Sanger sequencing (Supporting Information Fig. S1D). As shown in Supporting Information Fig. S1E, the DSB-induced indels resulted in complete loss of telomerase activity in these three ES cell clones. All three telomerase-null ES cell clones maintained normal karyotype (data not shown). However, these telomerase-null ES cells clones had short median telomeres approximately 5-6 kb (Supporting Information Fig. S1F, lanes 2-4). They could only be cultured for another 5-6 passages before cell proliferation loss and cell death induction, which is consistent with previous publication [38]. The cell death in these ES cell clones is distinct from primary fibroblasts that enter senescence when telomeres are critically short. The shortened proliferation capacity of telomerase-null ES cells limited their utility to understand ES cell responses to telomere dysfunction. To eliminate the possibility that the reduced proliferation lifespan of telomerase-null WA018 ES cells was due to

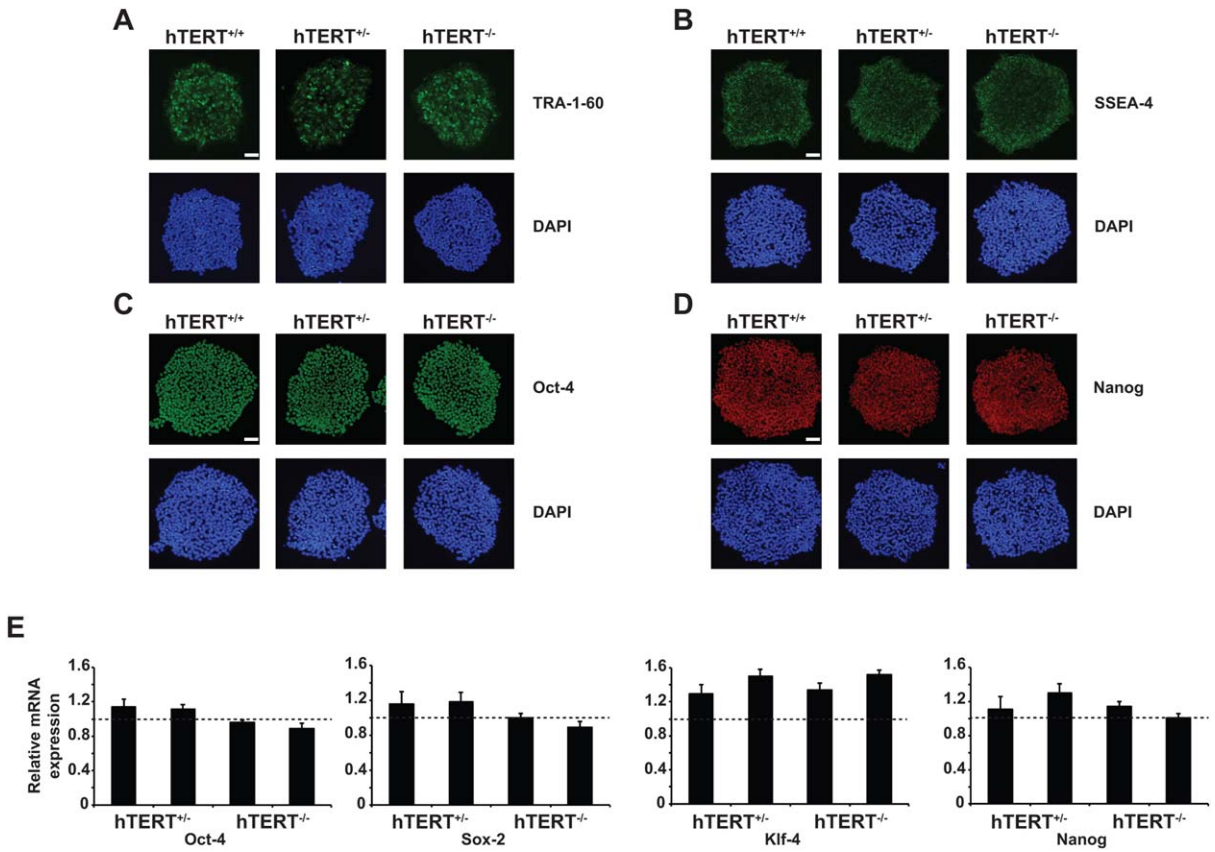

Figure 2. ES cell markers expression in *hTERT*-inducible knockout H1 embryonic stem (ES) cells. (A-D): Immunofluorescence staining analysis of TRA-1-60, SSEA-4, OCT-4, and NANOG in $hTERT^{+/+}$, $hTERT^{+/-}$, and $hTERT^{-/-}$ ES cells. The cell nuclei were stained with DAPI. Scale bar = 100 μM. (E): Expression of *OCT-4*, *SOX-2*, *KLF-4*, and *NANOG* in independent $hTERT^{+/+}$, $hTERT^{+/-}$, and $hTERT^{-/-}$ clonal ES cell lines quantified by qRT-PCR and normalized to *GAPDH* expression. The expression levels of *OCT-4*, *SOX-2*, *KLF-4*, and *NANOG* in parental $hTERT^{+/+}$ ES cells is indicated by the dotted line.

potential off-target effects of CRISPR/Cas9 system, we engineered telomerase-inducible knockout ES cells in different human ES cell lines (H1) using zinc finger nuclease (ZFN)-mediated gene targeting [34, 51–56]. Paired ZFNs were engineered to target distinct genomic DNA sequences in exon 1 of *hTERT* as shown in Supporting Information Figure S2. The expression of ZFNs in H1 ES cells resulted in site-specific DSBs in *hTERT* exon 1 with a low cutting efficiency (2%-3%) (Supporting Information Fig. S2B). So, we utilized ZFNs for gene targeting to create hTERT-inducible knockout human H1 ES cells. Our targeting vector introduced two loxP sites flanking *hTERT* exon 1 and exon 2 (Fig. 1A). Cre recombinase expression will result in the deletion of both exon 1 and exon 2 from the *hTERT* genomic locus, which encompasses almost 50% of the hTERT N-terminal protein coding region. To avoid cutting the targeting vector by coexpressed ZFNs during the gene targeting process, the ZFNs-binding sites on the targeting vector were mutated. These mutations resulted in a dramatic improvement in the stability of the full-length targeting vector (Supporting Information Fig. S3). Two rounds of gene targeting were performed to introduce loxP sites flanking both *hTERT* alleles (Supporting Information Fig. S4). The targeted *hTERT* alleles were confirmed through Southern blotting analysis (Fig. 1B). As shown by RNA protection assay (Fig. 1C), deletion of one *hTERT* copy ($hTERT^{+/-}$) resulted in a 50% loss of hTERT mRNA expression, while deletion of both hTERT copies ($hTERT^{-/-}$) yielded a complete loss of full-length *hTERT* mRNA expression in H1 ES cells. Consistent with the *hTERT* mRNA expression results, deletion of one allele of hTERT yielded an approximate 50% reduction of telomerase activity, and deletion of both alleles of *hTERT* resulted in a complete loss of telomerase activity (Fig. 1D) as determined by the TRAP assay [4]. Given the propensity of human ES cells to accumulate genetic aberrations during extended culture in vitro, karyotyping was done at each gene-targeting step to verify that the clonal-derived human ES cell lines maintain a normal karyotype (Supporting Information Fig. S5).

Stem Cell Marker Expression in Telomerase Knockout ES Cells

Like parental H1 ES cells ($hTERT^{+/+}$), the $hTERT^{+/-}$ and $hTERT^{-/-}$ ES cells expressed ES cell-specific surface antigens [57], such as TRA-1-60 and SSEA-4, and genes that maintain the undifferentiated ES cell state, such as OCT4 and NANOG (Fig. 2A-2D). Using qRT-PCR, expression levels of ES cell marker genes in $hTERT^{+/-}$ and $hTERT^{-/-}$ ES cells were comparable to parental H1 ES cells ($hTERT^{+/+}$), although there were small variations in different independent $hTERT^{+/-}$ and $hTERT^{-/-}$ clonal ES cell lines (Fig. 2E).

Progressive Telomere Shortening and Cell Proliferation Loss in Telomerase-Null ES Cells

Telomere length in parental H1 ES cells ($hTERT^{+/+}$) was ~13-14 kb determined through genomic Southern blotting analysis

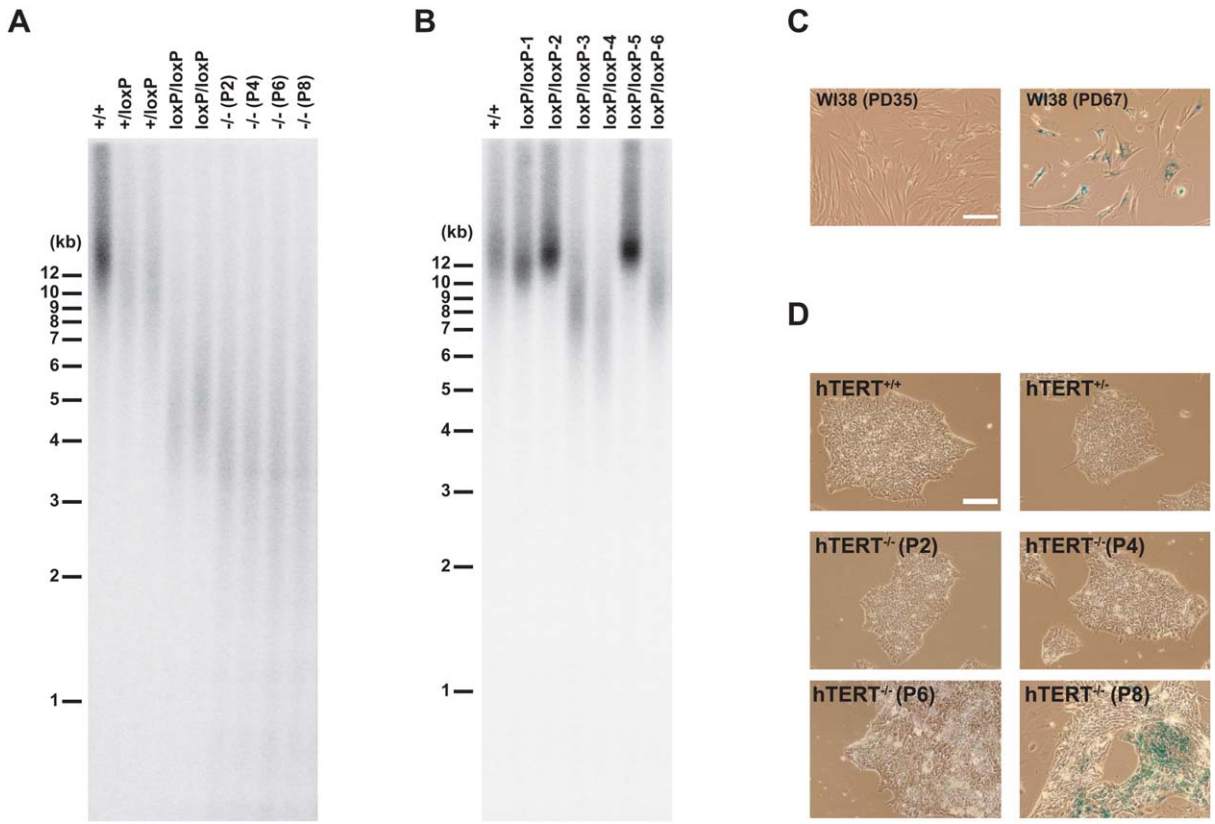

Figure 3. Telomere shortening in telomerase-null human embryonic stem (ES) cells. (A): Genomic Southern analysis of telomere length in independent *hTERT*$^{+/+}$, *hTERT*$^{+/loxP}$, *hTERT*$^{loxP/loxP}$, and *hTERT*$^{-/-}$ ES cell lines. (B): Transient hTERT overexpression resets telomere length in *hTERT*$^{loxP/loxP}$ ES cells. (C): Expression of senescence-associated β-galactosidase activity in young WI38 primary lung fibroblast cells (PD35) and senescent WI38 (PD67) cells. PD: population doubling. Scale bar = 100 μM. (D): Expression of senescence-associated β-galactosidase activity in late passage (P8) *hTERT*$^{-/-}$ ES cells. Scale bar = 100 μM.

(Fig. 3A). ES cells with loxP sites flanking only one *hTERT* allele (*hTERT*$^{+/loxP}$) showed slightly shortened telomeres compared to parental H1 ES cells. This was likely due to the disruption of *hTERT* expression by the neomycin-resistant gene cassette in the targeting vector (Fig. 1A) during the gene targeting process (Supporting Information Fig. S4). Introduction of loxP sites flanking exon 1 and exon 2 of *hTERT* also potentially inhibited *hTERT* mRNA expression. Consistent with this, further telomere shortening was observed in ES cell colonies with loxP sites flanking both alleles of hTERT (*hTERT*$^{loxP/loxP}$). As predicted, transient expression of Cre recombinase in *hTERT*$^{loxP/loxP}$ ES cells resulted in the loss of telomerase activity and gradual shortening of telomere length in *hTERT*$^{-/-}$ ES cells (Supporting Information Fig. 3A, P2-P8). Similar to telomerase-null ES cells derived from WA018 ES cell line, the *hTERT*$^{-/-}$ ES cell lines derived from H1 ES cell line could only be cultured for another ~8 passages (Fig. 3A) before cell proliferation loss and cell death induction.

Telomere Length Reset in Telomerase Inducible Knockout ES Cells by Transient hTERT Overexpression

Telomere length in *hTERT*$^{loxP/loxP}$ ES cells was maintained at a short and stable state (~5-6 kb) compared to parental H1 ES cells. These data indicate that telomerase activity in *hTERT*$^{loxP/loxP}$ ES cells was sufficient for telomere maintenance. These results also suggest that transient hTERT overexpression could boost telomerase activity and reset telomere length in *hTERT*$^{loxP/loxP}$ ES cells. To test this possibility, an episomal vector expressing hTERT-IRES-GFP was transiently transfected into *hTERT*$^{loxP/loxP}$ ES cells. Then, GFP-positive cells were FACS sorted, and single cell colonies were isolated. As shown in Figure 3B, single cell colonies derived from transient hTERT overexpression had elongated telomeres compared to their parental *hTERT*$^{loxP/loxP}$ ES cells. Several single cell-derived colonies have telomeres of similar length as the parental H1 ES cells. No integration of the hTERT-IRES-GFP expression vector was detected in these newly derived *hTERT*$^{loxP/loxP}$ ES cell colonies (data not shown). Accordingly, *hTERT*$^{-/-}$ ES cell colonies derived from these new *hTERT*$^{loxP/loxP}$ ES cells also had longer telomeres initially ~9-10 kb (Supporting Information Fig. S6). Such *hTERT*$^{-/-}$ ES cells could passage much longer than *hTERT*$^{-/-}$ ES cells with short telomeres (Fig. 3A), which permited an ample supply of telomerase-null ES cells for research and proof-of-principle applications.

Loss of Cell Proliferation Capacity and Increased Cell Death in Late Passage telomerase-Null ES Cells

When primary human fibroblast cells (WI38 PD67) entered a senescent state, cells were permanently arrested at G1 with enlarged cell morphology and positive staining for senescence-associated β-galactosidase as shown in Figure 3C [13, 58]. Similar to senescent primary fibroblast cells, *hTERT*$^{-/-}$ ES cells at late passage also showed increased expression of senescence-associated β-galactosidase activity (Fig. 3D). Celltiter-Glo luminescent cell

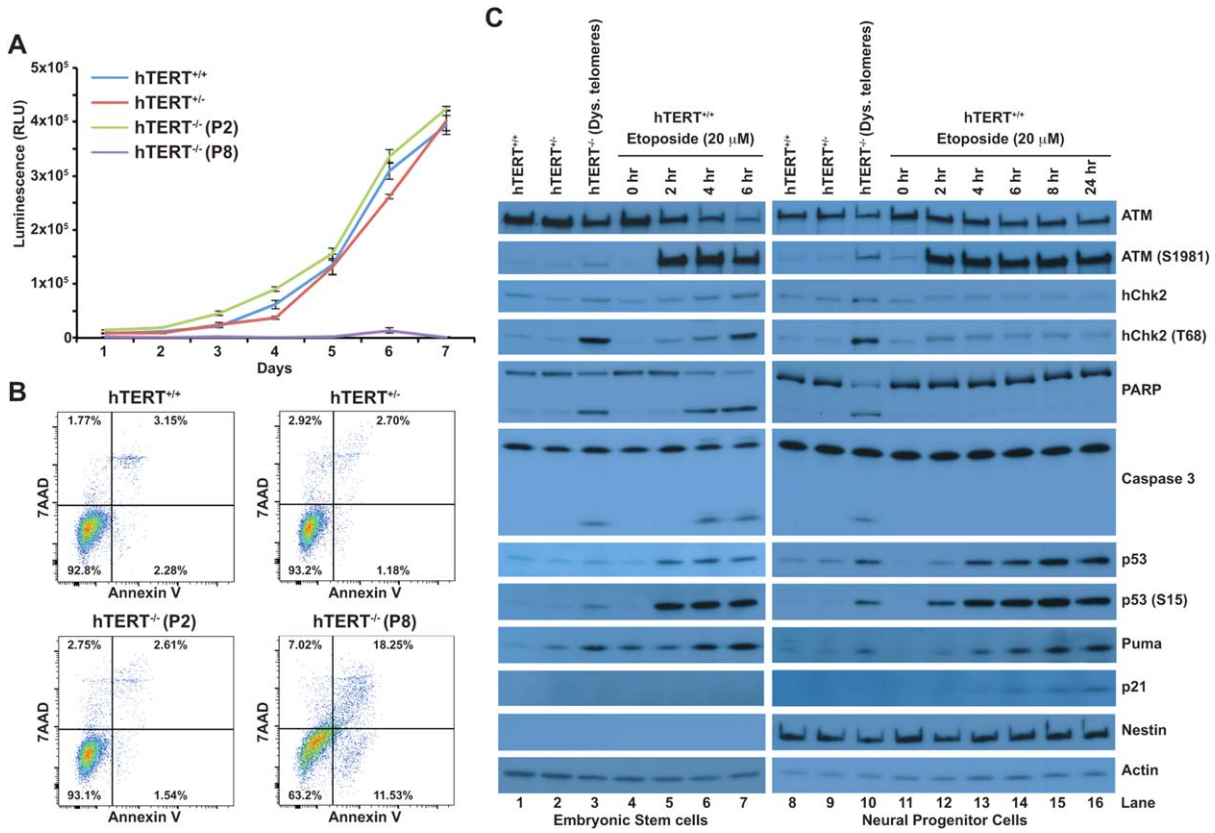

Figure 4. Cell proliferation loss and apoptosis induction in late passage $hTERT^{-/-}$ embryonic stem (ES) cells. (A): Cell viability measured using Celltiter-Glo luminescent assay in independent $hTERT^{+/+}$; $hTERT^{+/-}$, and $hTERT^{-/-}$ ES cell lines. (B): Annexin V and 7-AAD staining in independent $hTERT^{+/+}$; $hTERT^{+/-}$, and $hTERT^{-/-}$ ES cell lines. (C): Western blotting shows distinct DNA damage responses in human ES and neural progenitor cells (NPC) with dysfunctional telomeres- $hTERT^{-/-}$ (Dys. telomeres) as well as $hTERT^{+/+}$ human ES and NPC cells treated with 20 μM etoposide. Lanes 1-7: human ES cells. Lanes 8-16: human NPCs.

viability assay showed that $hTERT^{-/-}$ ES cells at early passage (P2 in Fig. 3A) had similar cell viability and cell proliferation rates compared to $hTERT^{+/+}$ and $hTERT^{+/-}$ ES cells (Fig. 4A). As shown in Supporting Information Figure S7A, cellular incorporation of EdU during S phase were comparable in $hTERT^{+/+}$, $hTERT^{+/-}$, and $hTERT^{-/-}$ (P2) ES cells. Cell cycle profile analysis also showed comparable G1, S, and G2/M cell cycle distribution in $hTERT^{-/-}$ (P2), $hTERT^{+/+}$, and $hTERT^{+/-}$ ES cells (Supporting Information Fig. S7B). However, $hTERT^{-/-}$ ES cells at late passage (P8 in Fig. 3A) lost proliferation potential (Fig. 4A), increased cell population at G1, and decreased cell population at G2/M phase. In addition to cell proliferation loss, Annexin V and 7-AAD staining showed increased apoptosis in $hTERT^{-/-}$ (P8) ES cells compared to $hTERT^{+/+}$, $hTERT^{+/-}$, and $hTERT^{-/-}$ (P2) ES cells (Fig. 4B). These results indicate that the cell proliferation capacity of ES cells was limited by telomere length in the absence of telomerase activity. When telomeres become critically short, stem cells lost proliferation capacity and induced apoptosis.

Distinct Stem Cell Responses to Telomere Uncapping and Etoposide Treatment

When telomeres become critically short, chromosomes become uncapped and develop distinct TIFs [10]. As shown in Supporting Information Figure S8, such TIFs (colocalization of γ-H2AX and Telomere FISH) occurred in the late passage $hTERT^{-/-}$ ES, while no TIFs were observed in ES cells treated with etoposide. To further characterize ES cells responses to telomere uncapping and genome-wide DNA damage, $hTERT^{+/+}$ ES cells were treated with 20 μM etoposide, and cellular responses were then compared to $hTERT^{-/-}$ ES cells (p8 with dysfunctional telomeres). As shown in Figure 4C (left panels), etoposide treatment resulted in a dramatic increase in ATM (S1981) phosphorylation. In contrast, telomere dysfunction in $hTERT^{-/-}$ (P8) ES cells resulted only in a slight increase in ATM (S1981) activation. However, Chk2 priming site (T68) phosphorylation was comparable in $hTERT^{-/-}$ (P8) ES cells with dysfunctional telomeres and $hTERT^{+/+}$ ES cells treated with 20 μM etoposide for 6 hours. As expected, p53 activation and Puma expression increased, but not p21 expression consistent with ES cells lacking the G1 checkpoint. Dramatic apoptosis induction was comparable in $hTERT^{-/-}$ (P8) ES cells with dysfunctional telomeres and $hTERT^{+/+}$ ES cells treated with 20 μM etoposide for 4 to 6 hours indicated by increased PARP and Caspase 3 cleavage products (Fig. 4C).

When $hTERT^{+/+}$ ES cells were induced to differentiate into NPCs for only three days, the partially differentiated NPCs, confirmed by Nestin expression, were no longer sensitive to etoposide-induced apoptosis demonstrated by the loss of Chk2 (T68) priming site phosphorylation, and PARP and Caspase 3 cleavages (Fig. 4C, right panels). In contrast, telomere dysfunction in partially differentiated NPCs still resulted in increased Chk2 (T68) priming site phosphorylation, and PARP and Caspase 3 cleavages. These results indicate that partially differentiated NPCs remain sensitive to telomere

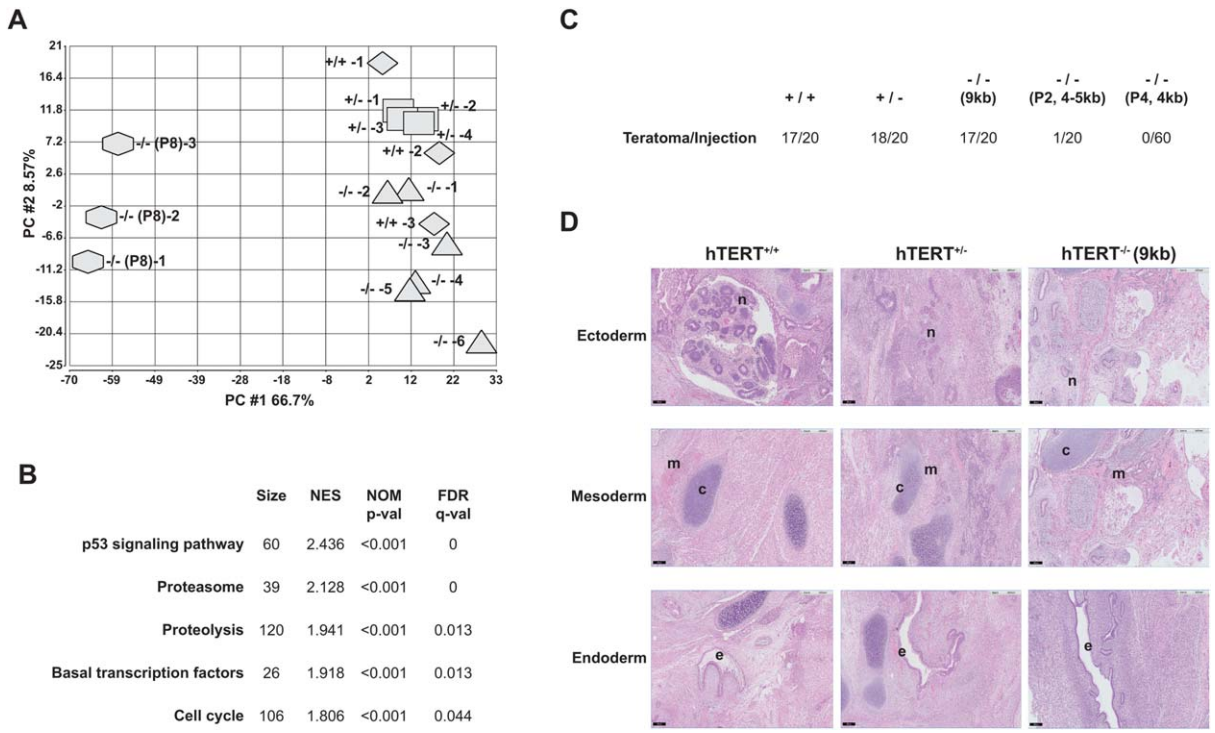

Figure 5. Gene expression-profiling and teratoma formation in vivo. (A): Principal components analysis of gene expression profiles in $hTERT^{+/+}$; $hTERT^{+/-}$, $hTERT^{-/-}$ (P2), and $hTERT^{-/-}$ (P8 with dysfunctional telomeres) ES cell lines. (B): Gene-set enrichment analysis of differentially expressed genes in $hTERT^{-/-}$ (P8 with dysfunctional telomeres) cell lines versus $hTERT^{+/+}$; $hTERT^{+/-}$, and $hTERT^{-/-}$ (P2) ES cell lines based on gene-sets from Kyoto Encyclopedia of Genes and Genomes. Only the top five pathways (sorted by NES) are shown. (C): Teratoma formation efficiency in independent $hTERT^{+/+}$; $hTERT^{+/-}$, and $hTERT^{-/-}$ ES cell lines. (D): H&E staining of teratomas derived from independent $hTERT^{+/+}$; $hTERT^{+/-}$, and $hTERT^{-/-}$ ES cell lines. Endoderm: respiratory epithelium (e); Mesoderm: cartilage (c) and skeletal muscle (m); Ectoderm: neural epithelium with rosettes (n). Scale bars = 200 μm. Abbreviations: FDR, false discovery rate; NES, normalized enrichment score; NOM *p* value, normalized *p* value.

dysfunction-induced apoptosis, while being resistant to etoposide treatment. These differences are likely due to the irreparable nature of telomere uncapping [11, 12]. These results also indicate that telomere shortening induced by telomerase inactivation in ES cells was effective in eliminating pluripotent stem cells and partially differentiated progenitor cells. This may improve the safety of stem cell therapies, as recent studies also indicated that partially differentiated progenitor cells can spontaneously regain pluripotency [59].

Genome-Wide Gene Expression Profiling of Telomerase-Null ES Cells

Previous studies found that hTERT has telomere-independent functions crucial for gene expression regulation, which may affect stem cell proliferation and survival [21, 60, 61]. To determine whether hTERT inactivation affects genome-wide gene expression, the gene expression profiles of $hTERT^{+/+}$, $hTERT^{+/-}$, $hTERT^{-/-}$ (P2), and $hTERT^{-/-}$ (P8 with dysfunctional telomeres) ES cells were analyzed by DNA microarray analysis. No significant differences in gene expression were observed in $hTERT^{+/+}$, $hTERT^{+/-}$ and $hTERT^{-/-}$ (P2) ES cells (Fig. 5A and Supporting Information Tables S1-S3). As expected, p53 DNA damage response activation and apoptosis induction was readily observed in $hTERT^{-/-}$ (P8 with dysfunctional telomeres) ES cells consistent with their telomeres being critically short (Fig. 5B, Supporting Information Fig. S9 and Table S4, S5). Previous results demonstrated that hTERT loss affects gene expression within *Wnt/β-catenin* pathway members [62]. However, results from our DNA microarray analysis did not show significant changes in gene expression profile in the *Wnt/β-catenin* pathway (Supporting Information Table S6). Interestingly, even when apoptosis was induced in late passage telomerase-null ES cells, most pluripotency genes were still expressed at similar levels compared to $hTERT^{+/+}$ ES cells (Supporting Information Table S7).

Telomerase-Null ES Cell Pluripotency

Next, we investigated whether inactivation of telomerase activity affects ES cell pluripotency. Loss of telomerase activity does not affect stem cell marker expression in independent $hTERT^{+/+}$, $hTERT^{+/-}$ and $hTERT^{-/-}$ ES cell lines (Fig. 2). To determine the differentiation potential of telomerase-null ES cells in vitro, these cells were grown in suspension to induce EBs formation [63]. The $hTERT^{+/+}$, $hTERT^{+/-}$ and $hTERT^{-/-}$ ES cells formed EB efficiently (data not shown). EBs were then plated on gelatin-coated plates and cultured for 2 weeks. The attached cells spontaneously differentiated into cell types representative of the three germ layers (Supporting Information Fig. S10) expressing early differentiation markers for ectoderm (Tuj1 and GFAP), mesoderm (SMA and Desmin), and endoderm (AFP). These data indicated that $hTERT^{-/-}$ ES cells are pluripotent. To further test $hTERT^{-/-}$ ES cell pluripotency in vivo, $hTERT^{+/+}$, $hTERT^{+/-}$ and $hTERT^{-/-}$ ES cells were injected subcutaneously into the dorsal-lateral area of immunodeficient NSG mice as previously described [45]. Eight weeks postinjection, teratoma formation was evaluated (Fig.

5C, 5D). Similar to $hTERT^{+/+}$ and $hTERT^{+/-}$ ES cells, $hTERT^{-/-}$ ES cells with long telomeres (~9 kb; P1 in Supporting Information Fig. S6) formed teratomas efficiently in immunodeficient mice. However, when $hTERT^{-/-}$ ES cells with shorter telomeres (~4-5 kb; P2 in Fig. 3A) were injected into immunodeficient mice, only 1 out of 20 injections resulted in teratoma formation. When $hTERT^{-/-}$ ES cells with even shorter telomeres (~4 kb, P4 in Fig. 3A) were injected into immunodeficient mice, no injection (0/60) resulted in teratoma formation in vivo. Consistent with these results, $hTERT^{-/-}$ ES cells with short telomeres (~4 kb; P4 in Fig. 3A) could only be cultured in vitro for another 4 passages. Histological examination of the tumors obtained from $hTERT^{+/+}$, $hTERT^{+/-}$, and $hTERT^{-/-}$ ES cells showed that these tumors contained various tissues derived from all three germ layers, including respiratory epithelium (endoderm), striated muscle and cartilage (mesoderm), and neural epithelium with rosettes (ectoderm) (Fig. 5D). No alternative lengthening of telomere (ALT) pathway activation in teratomas derived from $hTERT^{-/-}$ ES cells was observed (Supporting Information Fig. S11). These results indicated that telomerase activity inactivation does not affect ES cell pluripotency. However, the proliferation capacity of $hTERT^{-/-}$ ES cells and their ability to form teratomas in vivo is limited by telomere length, which presets their proliferation potential.

Neural Differentiation of telomerase-Null ES Cells In Vitro

We, then, tested whether $hTERT^{-/-}$ ES cells can differentiate into specific cell types using established protocols for human ES cell differentiation. Neural induction of $hTERT^{+/+}$; $hTERT^{+/-}$, and $hTERT^{-/-}$ ES cells was carried out as previously reported [44] (Supporting Information Fig. S12A). Immunofluorescence staining assays showed that NPCs derived from $hTERT^{+/+}$; $hTERT^{+/-}$, and $hTERT^{-/-}$ (~4 kb; P4 in Fig. 3A) ES cells were positive for Nestin and Sox2 staining (Supporting Information Fig. S12B). When NPCs were further induced to differentiate into either immature neurons or astrocytes, NPCs derived from $hTERT^{+/+}$; $hTERT^{+/-}$, and $hTERT^{-/-}$ ES cells showed similar ability to differentiate into DCX-positive immature neurons, as well as GFAP-positive glial cells (Supporting Information Fig. S12C-S12E).

Neural Differentiation of telomerase-Null ES Cells In Vivo

NPCs derived from human ES cells and iPS cells hold great promise for an array of neurodegenerative diseases, such as Parkinson's disease and Alzheimer's disease, and spinal cord injuries. However, injection of NPCs rather than terminally differentiated cells further raises the risk of tumor formation in vivo [64]. To determine whether newly engineered $hTERT^{-/-}$ ES cells offer additional advantages to reduce such safety risks, we injected $hTERT^{+/+}$ and $hTERT^{-/-}$ (~4 kb, P4 in Fig. 3A) ES cells directly into the midbrain of immunodeficient mice. DCX-positive human cells were detected in mouse brains that either received $hTERT^{+/+}$ or $hTERT^{-/-}$ ES cells four weeks after the injection as shown in Figure 6A-6D. However, brain sections of the mice that received $hTERT^{+/+}$ ES cell injections showed local proliferation and expansion of cell/tissue masses positive for human nuclei staining. These data indicate continuous proliferation of cells derived from $hTERT^{+/+}$ ES cells postinjection. At 16 weeks after injection, large tumors were observed in all five mice injected with human $hTERT^{+/+}$ ES cells (Fig. 6E, 6F). In contrast, no tumors were found in mice that were injected with $hTERT^{-/-}$ ES cells (Fig. 6E). Immunostaining indicated that injected $hTERT^{+/+}$ ES cells and $hTERT^{-/-}$ ES cells proliferated in vivo. However, the proliferation potential of $hTERT^{-/-}$ ES cells was restricted by their telomere length (Supporting Information Fig. S13). The injected $hTERT^{-/-}$ ES cells were viable and proliferating (Supporting Information Fig. S14A). MAP2a- (mature neuronal marker) and tyrosine hydroxylase (TH; a marker for mature dopaminergic neuron)-positive cells differentiated from $hTERT^{-/-}$ ES cells were detected 16 weeks after injection (Supporting Information Figure S14B, S14C). Lack of tumor formation in mice injected with $hTERT^{-/-}$ ES cells indicates that it is even less likely for the NPCs derived from human $hTERT^{-/-}$ ES cells to form tumor in vivo, thus provides improved safety for cell therapy in vivo.

Discussion

The ability of pluripotent stem cells to self-renew and to differentiate into various cell types from all three germ layers provides an unlimited resource for human cell therapy and disease modeling. However, they also proliferate continuously raising concerns for tumor formation in vivo, since pluripotent stem cells share cellular and genetic similarities with cancer cells [65]. These pluripotent stem cells can form teratomas as low as a few hundred when injected into immunodeficient mice [66, 67]. Since oncogenic characteristics of human pluripotent stem cells are so central to their identity, teratoma formation is the gold standard to demonstrate pluripotency of stem cells. There is a similar risk using partially differentiated progenitor cells, since they can regain pluripotency spontaneously [59]. Indeed, recent reports confirm that donor-derived tumors occur after allogeneic neural progenitor stem cell [64] and autologous hematopoietic stem cell transplantations [68]. These reports propose strategy developments to reduce and overcome the tumorigenicity risk of pluripotent stem cells. These strategies entail eliminating residual pluripotent stem cells from differentiated cells and using suicide genes [69–71]. While these strategies show promise, major limitations still persist. For example, technological challenges exist to completely separate differentiated cells from residual pluripotent stem cells. These methods may not completely eliminate partially differentiated progenitor cells, as DNA damage agents are not effective to purge partially differentiated progenitor cells. Recent clinical trials utilizing suicide genes, such as HSV-TK and FKBP-caspase 9, elicit immunogenicity in patients and incomplete elimination of targeted cells respectively [70, 71]. In addition to these obstacles, cell therapy poses further complications to implement these strategies, since high number of cells (up to hundreds of thousands) may be necessary for each cell therapy. Differentiated cells derived from pluripotent stem cells may also acquire secondary genetic mutations leading to malignant transformations during cell culture in vitro. Prolonged culture of pluripotent stem cells in vitro can produce various genomic abnormalities including chromosomal translocations and aneuploidy, subchromosomal duplication and deletion, and point mutations [72]. Therefore, the technical burden of separating differentiated cells from

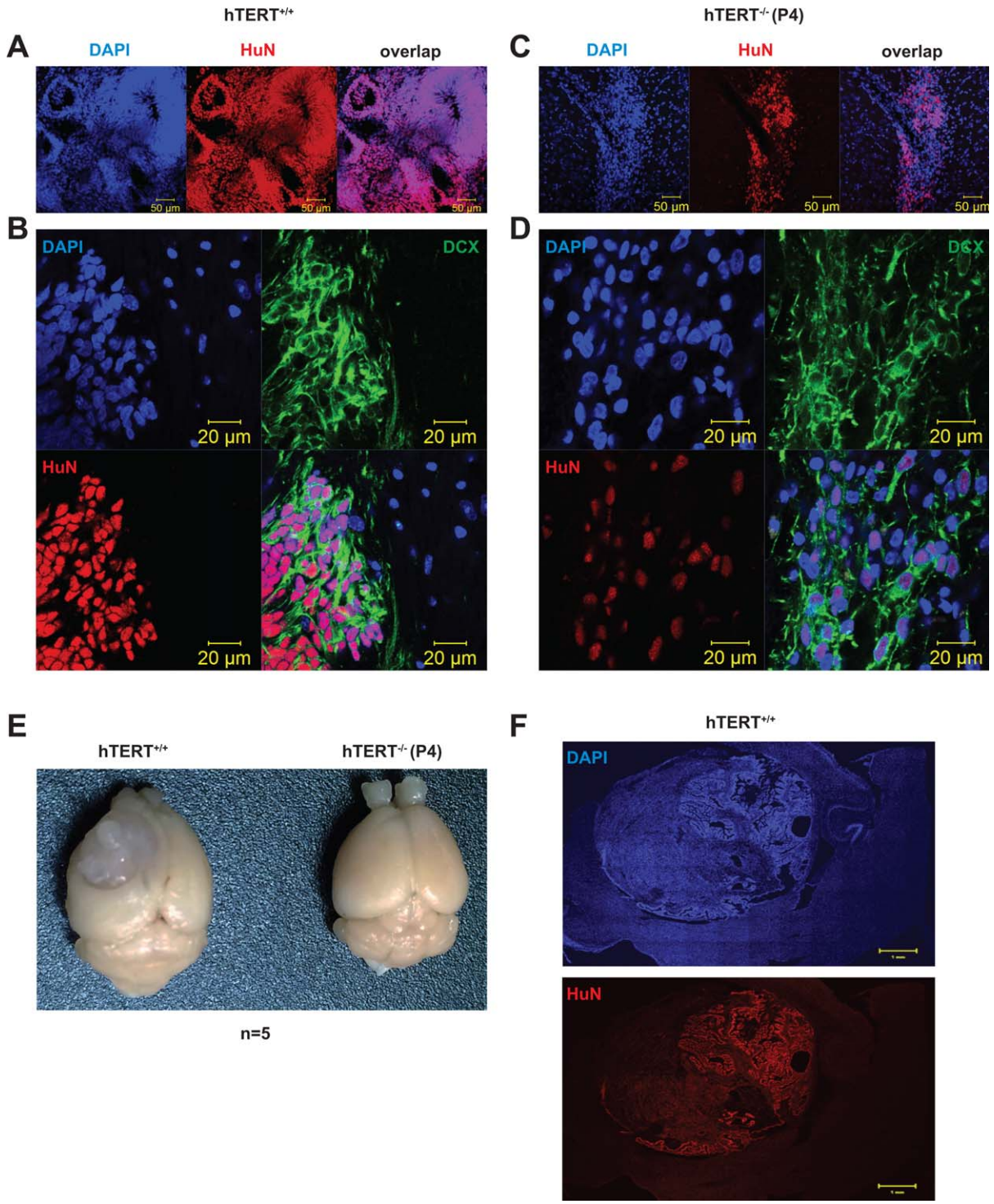

Figure 6. Implantation of telomerase-null human ES cells in vivo. (A and B): Representative images showing immunofluorescence staining of mouse brain sections from mice injected with $hTERT^{+/+}$ ES cells. (C and D): Representative images showing immunofluorescence staining of mouse brain sections from mice injected with $hTERT^{-/-}$ ES cells. (E): Gross morphology of brains from mice injected with $hTERT^{+/+}$ ES cells or $hTERT^{-/-}$ ES cells. Tumor formation was visible in $hTERT^{+/+}$ ES but not $hTERT^{-/-}$ ES-injected mouse brains. The number of mice injected with $hTERT^{+/+}$ ES cells or $hTERT^{-/-}$ ES cells ($n = 5$). (F): Representative confocal images showing HuN staining of tumors in $hTERT^{+/+}$ ES cells-injected mice. Scale bar = 1mm. Abbreviations: HuN, human nuclei.

undifferentiated pluripotent stem cells and ensuring the genetic stability of differentiated cells remains a major challenge for widespread applications of clinical cell therapy.

Our results suggest that inactivation of telomerase activity through hTERT knockout in ES cells limits the self-renewal capacity of stem cells. We further demonstrated that *hTERT* inactivation does not alter ES cell pluripotency using in vitro and

in vivo assays. When telomeres shorten to a critical limit approximately 3-4 kb, ES cells trigger DNA damage response-induced apoptosis. Partially differentiated NPCs are also sensitive to dysfunctional telomeres. This is significant, since these NPCs are resistant to etoposide-induced apoptosis. The irreparable nature of telomere DNA damage [11, 12] may play a role in stimulating NPC apoptosis. Consistent with these results, telomerase-null ES cells also lost the ability to form teratomas in vivo when their telomeres reach approximately 4 kb as measured by teloblot. Since telomere dysfunction is induced by critically short telomeres and individual telomere length in ES cells can be longer or shorter than 4 kb, a more accurate method for telomere length measurement, such as STELA [73], may be advantageous to select clonal telomerase-null ES cells for in vivo cell therapy in the future. By selecting telomerase-null ES cells with shorter telomere lengths, we can potentially reduce the tumor formation risk for in vivo cell therapy.

Telomerase activity is significantly elevated in more than 85%-90% of all human cancers and in over 70% of immortalized human cell lines [4, 74, 75]. Telomerase activity upregulation in cancer cells is necessary for telomere maintenance and continuous cancer cell division. Blocking telomere maintenance through inactivating telomerase activity also reduces the tumorigenicity risk of progenitor cells derived from ES cells that acquired secondary genetic mutations, which may promote *hTERT* activation and cell immortalization in vivo. Telomere length can be sustained in telomerase-negative cells by activating ALT mechanisms [76]. However, we did not observe any spontaneous emergence of ALT survivors from telomerase-null human ES cells in vitro and in vivo (Supporting Information Fig. S11). Additional mutations and factors may be necessary to activate the ALT pathway in telomerase-null human ES cells. Therefore, our results suggest that substantial reductions in tumor formation risk from pluripotent stem cells occur through restricting telomere maintenance mechanisms in vivo.

Given that telomerase expression is naturally silenced during somatic tissue differentiation [4, 74], telomerase is likely dispensable for normal cellular functions in terminally differentiated cells. This prediction is supported by observations that telomerase knockout mice are viable, fertile, and relatively normal through the first 2-3 generations, due to the extremely long telomeres in laboratory mice [24, 46–49]. Further, our data indicate that no dramatic differences in cell proliferation and cell viability in $hTERT^{+/+}$, $hTERT^{+/-}$, and $hTERT^{-/-}$ ES cells exist prior to the onset of telomere dysfunction-induced DNA damage responses. No substantial differences were observed in genome-wide gene expression profile analyses of $hTERT^{+/+}$, $hTERT^{+/-}$, and $hTERT^{-/-}$ ES cells before telomeres shortened to a critical length (Supporting Information Tables S1-S5).

For stem cell-based cell transplantation applications using terminally differentiated cells, such as retinal pigment cells and specific progenitor cells, such as NPCs and mesenchymal stem cells, telomerase-null ES cells will be useful as these cells do not require sustained cell proliferation in vivo indicating that they do not need sustained telomerase activity. By tailoring telomere length in telomerase-null ES cells, we can predict and can limit the proliferation capacity of progenitor cells derived from telomerase-null ES cells. Therefore, this strategy provides a solution to balance the capacity of cell proliferation and the prevention of tumor formation.

Conclusions

This study demonstrates that telomerase is dispensable for ES cell pluripotency. Further, our results provide a potential strategy to improve the safety of cell therapy through telomerase inactivation, which inhibits tumor formation in vivo.

Acknowledgments

We thank Dr. Alvin Lim and Dr. Su Keyau Kee for their assistance with karyotyping of human ES cells. We thank Dr. Tony Kiat Hon Lim for his assistance with the H&E staining of teratomas. We thank life science editors for editing services. This work was supported by grants from NMRC and MOE tier 2 funding (Singapore) to S.L.

Author Contributions

C.C.L.: Engineered, characterized, and studied hTERT KO cells; D.M.: Performed differentiation of hES cells, transplantation and in vivo characterization; T.Y.: Characterized and studied hTERT KO cells; X.F., Z.P., L.P., and S.G.: Collection of data. S.G.R., W.H., V.T., P.T., S.G., D.M.V., and E.G.: Performed data analysis and interpretation; S.L.: Conception and design, financial support, manuscript writing, and final approval of the manuscript.

Disclosure of Potential Conflict of Interest

The authors indicate no potential conflicts of interest.

References

1 Palm W, de Lange T. How shelterin protects mammalian telomeres. Annu Rev Genet 2008;42:301–334.

2 Feng J, Funk WD, Wang SS et al. The RNA component of human telomerase. Science 1995;269:1236–1241.

3 Nakamura TM, Morin GB, Chapman KB et al. Telomerase catalytic subunit homologs from fission yeast and human. Science 1997; 277:955–959.

4 Kim NW, Piatyszek MA, Prowse KR et al. Specific association of human telomerase activity with immortal cells and cancer. Science 1994;266:2011–2015.

5 Masutomi K, Yu EY, Khurts S et al. Telomerase maintains telomere structure in normal human cells. Cell 2003;114:241–253.

6 Wright WE, Piatyszek MA, Rainey WE et al. Telomerase activity in human germline and embryonic tissues and cells. Dev Genet 1996;18:173–179.

7 Levy MZ, Allsopp RC, Futcher AB et al. Telomere end-replication problem and cell aging. J Mol Biol 1992;225:951–960.

8 Wright WE, Tesmer VM, Huffman KE et al. Normal human chromosomes have long G-rich telomeric overhangs at one end. Genes Dev 1997;11:2801–2809.

9 Harley CB, Futcher AB, Greider CW. Telomeres shorten during ageing of human fibroblasts. Nature 1990;345:458–460.

10 Takai H, Smogorzewska A, de Lange T. DNA damage foci at dysfunctional telomeres. Curr Biol 2003;13:1549–1556.

11 Fumagalli M, Rossiello F, Clerici M et al. Telomeric DNA damage is irreparable and causes persistent DNA-damage-response activation. Nat Cell Biol 2012;14:355–365.

12 Hewitt G, Jurk D, Marques FD et al. Telomeres are favoured targets of a persistent DNA damage response in ageing and stress-induced senescence. Nat Commun 2012;3:708.

13 Hayflick L Moorhead PS. The serial cultivation of human diploid cell strains. Exp Cell Res 1961;25:585–621.
14 d'Adda D, Fagagna F, Reaper PM, et al. A DNA damage checkpoint response in telomere-initiated senescence. Nature 2003;426:194–198.
15 Kaul Z, Cesare AJ, Huschtscha LI et al. Five dysfunctional telomeres predict onset of senescence in human cells. EMBO Rep 2012; 13:52–59.
16 Campisi J D'adda, di Fagagna F. Cellular senescence: When bad things happen to good cells. Nat Rev Mol Cell Biol 2007;8: 729–740.
17 Shay JW, Pereira-Smith OM, Wright WE. A role for both RB and p53 in the regulation of human cellular senescence. Exp Cell Res 1991;196:33–39.
18 Brown JP, Wei W, Sedivy JM. Bypass of senescence after disruption of p21CIP1/WAF1 gene in normal diploid human fibroblasts. Science 1997;277:831–834.
19 Cesare AJ, Karlseder J. A three-state model of telomere control over human proliferative boundaries. Curr Opin Cell Biol 2012;24:731–738.
20 Flores I, Canela A, Vera E et al. The longest telomeres: A general signature of adult stem cell compartments. Genes Dev 2008;22: 654–667.
21 Artandi SE, DePinho RA. Telomeres and telomerase in cancer. Carcinogenesis 2010; 31:9–18.
22 Lansdorp PM. Telomeres and disease. EMBO J 2009;28:2532–2540.
23 Blasco MA, Lee HW, Hande MP et al. Telomere shortening and tumor formation by mouse cells lacking telomerase RNA. Cell 1997;91:25–34.
24 Lee HW, Blasco MA, Gottlieb GJ et al. Essential role of mouse telomerase in highly proliferative organs. Nature 1998;392:569–574.
25 Hao LY, Armanios M, Strong MA et al. Short telomeres, even in the presence of telomerase, limit tissue renewal capacity. Cell 2005;123:1121–1131.
26 Filion TM, Qiao M, Ghule PN et al. Survival responses of human embryonic stem cells to DNA damage. J Cell Physiol 2009;220: 586–592.
27 Grandela C, Pera MF, Grimmond SM et al. p53 is required for etoposide-induced apoptosis of human embryonic stem cells. Stem Cell Res 2007;1:116–128.
28 Momcilovic O, Choi S, Varum S et al. Ionizing radiation induces ataxia telangiectasia mutated-dependent checkpoint signaling and G(2) but not G(1) cell cycle arrest in pluripotent human embryonic stem cells. Stem Cells 2009;27:1822–1835.
29 Qin H, Yu T, Qing T et al. Regulation of apoptosis and differentiation by p53 in human embryonic stem cells. J Biol Chem 2007;282:5842–5852.
30 Liu JC, Guan X, Ryan JA et al. High mitochondrial priming sensitizes hESCs to DNA-damage-induced apoptosis. Cell Stem Cell 2013;13:483–491.
31 Dumitru R, Gama V, Fagan BM et al. Human embryonic stem cells have constitutively active Bax at the Golgi and are primed to undergo rapid apoptosis. Mol Cell 2012; 46:573–583.
32 Mandal PK, Blanpain C Rossi DJ. DNA damage response in adult stem cells: Pathways and consequences. Nat Rev Mol Cell Biol 2011;12:198–202.
33 Ran FA, Hsu PD, Wright J et al. Genome engineering using the CRISPR-Cas9 system. Nat Protoc 2013;8:2281–2308.
34 Soldner F, Laganiere J, Cheng AW et al. Generation of isogenic pluripotent stem cells differing exclusively at two early onset Parkinson point mutations. Cell 2011;146:318–331.
35 Ramlee MK, Yan T, Cheung AM et al. High-throughput genotyping of CRISPR/Cas9-mediated mutants using fluorescent PCR-capillary gel electrophoresis. Sci Rep 2015;5: 15587.
36 Zhang X, Guo C, Chen Y et al. Epitope tagging of endogenous proteins for genome-wide ChIP-chip studies. Nat Methods 2008;5: 163–165.
37 Liu CY, Flesken-Nikitin A, Li S et al. Inactivation of the mouse Brca1 gene leads to failure in the morphogenesis of the egg cylinder in early postimplantation development. Genes Dev 1996;10:1835–1843.
38 Sexton AN, Regalado SG, Lai CS et al. Genetic and molecular identification of three human TPP1 functions in telomerase action: Recruitment, activation, and homeostasis set point regulation. Genes Dev 2014;28:1885–1899.
39 Irizarry RA, Bolstad BM, Collin F et al. Summaries of Affymetrix GeneChip probe level data. Nucleic Acids Res 2003;31:e15.
40 Storey JD, Tibshirani R. Statistical significance for genomewide studies. Proc Natl Acad Sci USA 2003;100:9440–9445.
41 Subramanian A, Tamayo P, Mootha VK et al. Gene set enrichment analysis: A knowledge-based approach for interpreting genome-wide expression profiles. Proc Natl Acad Sci USA 2005;102:15545–15550.
42 Liberzon A. A description of the Molecular Signatures Database (MSigDB) Web site. Methods Mol Biol 2014;1150:153–160.
43 Dimos JT, Rodolfa KT, Niakan KK et al. Induced pluripotent stem cells generated from patients with ALS can be differentiated into motor neurons. Science 2008;321:1218–1221.
44 Li W, Sun W, Zhang Y et al. Rapid induction and long-term self-renewal of primitive neural precursors from human embryonic stem cells by small molecule inhibitors. Proc Natl Acad Sci USA 2011;108:8299–8304.
45 Prokhorova TA, Harkness LM, Frandsen U et al. Teratoma formation by human embryonic stem cells is site dependent and enhanced by the presence of Matrigel. Stem Cells Dev 2009;18:47–54.
46 Chiang YJ, Hemann MT, Hathcock KS et al. Expression of telomerase RNA template, but not telomerase reverse transcriptase, is limiting for telomere length maintenance in vivo. Mol Cell Biol 2004;24: 7024–7031.
47 Liu Y, Snow BE, Hande MP et al. The telomerase reverse transcriptase is limiting and necessary for telomerase function in vivo. Curr Biol 2000;10:1459–1462.
48 Yuan X, Ishibashi S, Hatakeyama S et al. Presence of telomeric G-strand tails in the telomerase catalytic subunit TERT knockout mice. Genes Cells 1999;4:563–572.
49 Strong MA, Vidal-Cardenas SL, Karim B et al. Phenotypes in mTERT(+)/(-) and mTERT(-)/(-) mice are due to short telomeres, not telomere-independent functions of telomerase reverse transcriptase. Mol Cell Biol 2011;31:2369–2379.
50 Ran FA, Hsu PD, Lin CY et al. Double nicking by RNA-guided CRISPR Cas9 for enhanced genome editing specificity. Cell 2013;154:1380–1389.
51 Jasin M. Genetic manipulation of genomes with rare-cutting endonucleases. Trends Genet 1996;12:224–228.
52 van der Oost J. Molecular biology. New tool for genome surgery. Science 2013;339: 768–770.
53 Boch J, Scholze H, Schornack S et al. Breaking the code of DNA binding specificity of TAL-type III effectors. Science 2009;326: 1509–1512.
54 Moscou MJ, Bogdanove AJ. A simple cipher governs DNA recognition by TAL effectors. Science 2009;326:1501.
55 Kim YG, Cha J, Chandrasegaran S. Hybrid restriction enzymes: zinc finger fusions to Fok I cleavage domain. Proc Natl Acad Sci USA 1996;93:1156–1160.
56 Bibikova M, Beumer K, Trautman JK et al. Enhancing gene targeting with designed zinc finger nucleases. Science 2003;300:764.
57 Adewumi O, Aflatoonian B, Ahrlund-Richter L et al. Characterization of human embryonic stem cell lines by the International Stem Cell Initiative. Nat Biotechnol 2007;25:803–816.
58 Dimri GP, Lee X, Basile G et al. A biomarker that identifies senescent human cells in culture and in aging skin in vivo. Proc Natl Acad Sci USA 1995;92:9363–9367.
59 Choi HW, Kim JS, Choi S et al. Neural stem cells differentiated from iPS cells spontaneously regain pluripotency. Stem Cells 2014;32:2596–2604.
60 Ye J, Renault VM, Jamet K et al. Transcriptional outcome of telomere signalling. Nat Rev Genet 2014;15:491–503.
61 Li Y, Tergaonkar V. Noncanonical functions of telomerase: Implications in telomerase-targeted cancer therapies. Cancer Res 2014;74:1639–1644.
62 Park JI, Venteicher AS, Hong JY et al. Telomerase modulates Wnt signalling by association with target gene chromatin. Nature 2009;460:66–72.
63 Itskovitz-Eldor J, Schuldiner M, Karsenti D et al. Differentiation of human embryonic stem cells into embryoid bodies compromising the three embryonic germ layers. Mol Med 2000;6:88–95.
64 Amariglio N, Hirshberg A, Scheithauer BW et al. Donor-derived brain tumor following neural stem cell transplantation in an ataxia telangiectasia patient. PLoS Medicine 2009;6:e1000029.
65 Baker DE, Harrison NJ, Maltby E et al. Adaptation to culture of human embryonic stem cells and oncogenesis in vivo. Nat Biotechnol 2007;25:207–215.
66 Lee AS, Tang C, Cao F et al. Effects of cell number on teratoma formation by human embryonic stem cells. Cell Cycle 2009;8:2608–2612.

67 Hentze H, Soong PL, Wang ST et al. Teratoma formation by human embryonic stem cells: evaluation of essential parameters for future safety studies. Stem Cell Res 2009;2: 198–210.

68 Thirabanjasak D, Tantiwongse K Thorner PS. Angiomyeloproliferative lesions following autologous stem cell therapy. JASN 2010;21: 1218–1222.

69 Ben-David U Benvenisty N. The tumorigenicity of human embryonic and induced pluripotent stem cells. Nat Rev Cancer 2011; 11:268–277.

70 Bonini C, Bondanza A, Perna SK et al. The suicide gene therapy challenge: How to improve a successful gene therapy approach. Mol Ther 2007;15:1248–1252.

71 Jones BS, Lamb LS, Goldman F et al. Improving the safety of cell therapy products by suicide gene transfer. Front Pharmacol 2014;5:254.

72 Mayshar Y, Ben-David U, Lavon N et al. Identification and classification of chromosomal aberrations in human induced pluripotent stem cells. Cell Stem Cell 2010;7:521–531.

73 Baird DM, Rowson J, Wynford-Thomas D et al. Extensive allelic variation and ultrashort telomeres in senescent human cells. Nat Genet 2003;33:203–207.

74 Shay JW Bacchetti S. A survey of telomerase activity in human cancer. Eur J Cancer 1997;33:787–791.

75 Bernardes de Jesus B, Blasco MA. Telomerase at the intersection of cancer and aging. Trends Genet 2013;29:513–520.

76 Cesare AJ, Reddel RR. Alternative lengthening of telomeres: Models, mechanisms and implications. Nat Rev Genet 2010; 11:319–330.

See www.StemCells.com for supporting information available online.